available at www.sciencedirect.com

ScienceDirect

journal homepage: www.elsevier.com/locate/chnjc

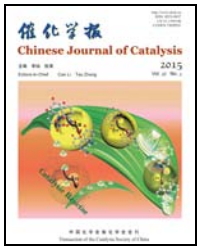

Article

Hydrothermal synthesis and photocatalytic properties of tantalum pentoxide nanorods

Juxia Li, Weili Dai *, Junqing Yan, Guangjun Wu, Landong Li, Naijia Guan #

Key Laboratory of Advanced Energy Materials Chemistry (Ministry of Education), College of Chemistry, Nankai University, Tianjin 300071, China

ARTICLE INFO

Article history:
Received 24 July 2014
Accepted 29 August 2014
Published 20 March 2015

Keywords:
Tantalum pentoxide
Nanostructure
Crystal growth
Photocatalytic property
Anisotropic growth

ABSTRACT

Tantalum pentoxide (Ta_2O_5) nanorods were hydrothermally synthesized using polyethylene glycol (PEG) as a guiding agent. The nanorods were characterized by X-ray diffraction, scanning and transmission electron microscopies, and diffuse reflectance ultraviolet-visible and photoluminescence spectroscopies. The effects of crystallization duration and Ta_2O_5/$Sr(OH)_2$ ratio on the product morphology were investigated, and a growth mechanism was proposed. Phase-pure Ta_2O_5 nanorods with controlled morphology were formed in the presence of PEG and $Sr(OH)_2$, which was necessary to form the nanorods. $Sr(OH)_2$ induced the surface dissolution and re-growth of Ta_2O_5. PEG induced the anisotropic growth of Ta_2O_5 by acting as a capping agent. The products were used to photocatalytically degrade rhodamine B under ultraviolet irradiation. The catalytic activity directly correlated with the length-diameter ratio of the Ta_2O_5 nanorods. A maximum apparent reaction rate constant of 0.156 min^{-1} was obtained. The Ta_2O_5 nanorods were stable during photocatalytic reaction and could be recycled several times without loss of activity.

1. Introduction

Semiconductor photocatalysis has attracted much interest for its potential in air pollution, solid waste and water pollution treatments [1–4]. Various semiconductors have been explored, with tantalum pentoxide (Ta_2O_5) being attractive because of its high photocatalytic activity, dielectric constant, refractive index, and chemical stability [5–10]. Nanomaterials with well-defined crystal structures and morphologies have been applied in various areas because of their size and structure-dependent properties [11–13]. Much effort has focused on one-dimensional (1D) nanostructures, such as nanorods and nanowires [14–24]. These exhibit different physical and chemical properties to their bulk counterparts.

Nanoparticulate Ta_2O_5 has been prepared by sol-gel [25,26], hydrothermal [27–29], solvothermal [30,31], hot filament metal vapor deposition [32], and microemulsion [33,34] methods. Most of these methods yield poorly crystalline Ta_2O_5 nanoparticles. Subsequent high-temperature calcination is also generally required to yield the final product, which can lower the surface area and decrease the catalytic activity. Hydrothermal synthesis can yield nanostructures with high crystallinity, high purity and narrow size distribution [35]. The product morphology can be controlled by adjusting the hydrothermal synthesis conditions. A few tantalates have been hydrothermally prepared at low temperature [36–41]. The hydrothermal synthesis of nanoparticulate Ta_2O_5 is difficult because Ta_2O_5 is much more inert than TiO_2 [34,42]. Ta_2O_5 nanowires [27] and nanoflowers [28] were recently hydrothermally prepared using hydrofluoric acid, which is impractical for green syntheses and

* Corresponding author. Tel: +86-22-23509140; Fax: +86-22-23500341; E-mail: weilidai@nankai.edu.cn
# Corresponding author. Tel: +86-22-23509140; Fax: +86-22-23500341; E-mail: guannj@nankai.edu.cn
This work was supported by the Collaborative Innovation Center of Chemical Science and Engineering (Tianjin).
DOI: 10.1016/S1872-2067(14)60215-1 | http://www.sciencedirect.com/science/journal/18722067 | Chin. J. Catal., Vol. 36, No. 3, March 2015

industrial application. Gömpel et al. [29] hydrothermally prepared Ta_2O_5 nanorods without using hydrofluoric acid, instead using an expensive tantalum(V) *n*-butoxide source. A hydrothermal synthesis of Ta_2O_5 nanoparticles using an economical Ta source in the absence of hydrofluoric acid is required.

In the present study, 1D Ta_2O_5 nanorods with tunable morphology were hydrothermally synthesized with the assistance of polyethylene glycol (PEG) and $Sr(OH)_2$. Ta_2O_5 powder was used as the Ta source. The effect of the synthesis parameters on the product morphology was investigated, and a growth mechanism was proposed. The photocatalytic performance of the Ta_2O_5 nanorods in the photodegradation of rhodamine B (RhB) under UV irradiation was investigated. The nanorods exhibited high activity, a high apparent reaction rate constant, and good recyclability.

2. Experimental

2.1. Hydrothermal synthesis of Ta_2O_5 nanorods

All chemicals were purchased from Alfa Aesar and used as received. In a typical synthesis, 2 mmol of Ta_2O_5 powder (99.99%) was dispersed in anhydrous ethanol, and a solution of $Sr(OH)_2$ was added dropwise under stirring. PEG (M_w = 300, 50 mg) with certain deionized water was added. The mixture was transferred to a polytetrafluoroethylene-lined autoclave (30 mL) for static crystallization at 200 °C for 5, 24, or 48 h. The resulting precipitate was collected by centrifugation and thoroughly washed with deionized water and ethanol. The product was dried at 80 °C overnight to yield Ta_2O_5 nanorods, which were denoted by Ta_2O_5-*x*-*y*, where *x* is the $Ta_2O_5/Sr(OH)_2$ molar ratio used during synthesis, and y is the reaction duration.

2.2. Characterization

X-ray diffraction (XRD) patterns were recorded on a Bruker D8 ADVANCE powder diffractometer using Cu-K_α radiation (λ = 0.1542 nm) at a scanning rate of 12°/min at 2θ = 10°–80°. Specific surface areas were determined through low-temperature N_2 adsorption-desorption isotherms, collected on a Quantachrome iQ-MP gas adsorption analyzer. Samples were dehydrated at 300 °C for 2 h prior to measurement. The total surface area was calculated via the BET equation. The morphologies and compositions were examined by field emission scanning electron microscopy (FE-SEM, Hitachi S-4800). Transmission electron microscopy (TEM) and high-resolution TEM (HRTEM) images were collected on a Philips Tecnai G2 20 S-TWIN microscope at 200 kV. A few drops of a sample suspension in ethanol were allowed to evaporate on a carbon-coated copper grid at ambient temperature. Ultraviolet-visible (UV-vis) diffuse reflectance spectra were recorded in the air against $BaSO_4$ at 200–700 nm using a Varian Cary 300 spectrophotometer. Photoluminescence (PL) spectra were recorded on a Spex FL201 fluorescence spectrophotometer. Samples were dry-pressed into self-supporting wafers and then excited by a 325-nm He–Cd laser at ambient temperature.

2.3. Photocatalytic degradation of RhB

The photocatalytic degradation of RhB was performed in a top-irradiation-type double-walled quartz cell cooled by water. A 250 W mercury lamp (λ_{max} = 365 nm) was used as the light source. About 0.1 g of catalyst was added to 200 mL of RhB solution (10 mg/L) in the quartz cell. The suspension was stirred in the dark until the RhB concentration was constant (~30 min), which indicated adsorption equilibrium. After commencing the photocatalytic reaction, aliquots were removed at regular time intervals and analyzed by UV-vis absorption spectrometry (Varian Cary 300).

3. Results and discussion

3.1. Effect of synthesis parameters on product morphology

The presence of PEG and $Sr(OH)_2$ during the hydrothermal synthesis of Ta_2O_5 nanostructures affects their resulting morphology. Figure 1 shows that irregular nanoparticles of large (~2 μm) and small (~200 nm) size were formed in the absence

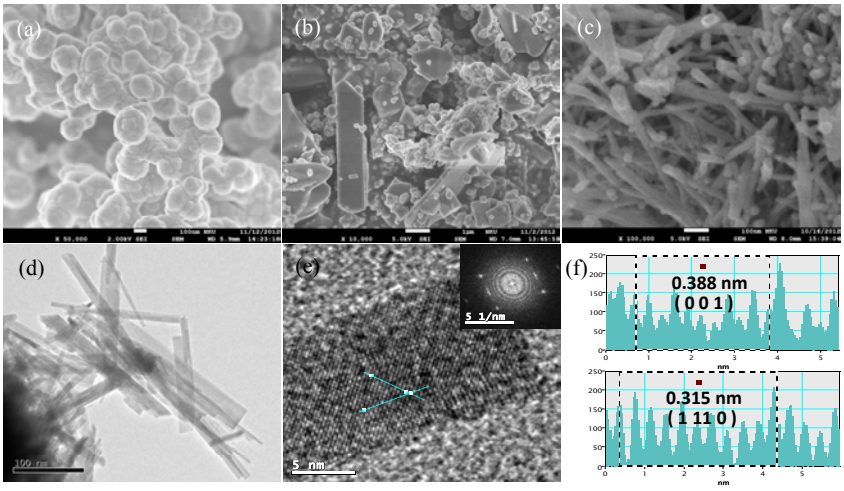

Fig. 1. SEM image of raw material Ta_2O_5 (a), synthesis product without PEG (b), and synthesis product with PEG (c); TEM (d) and HRTEM (e) images of synthesis product with PEG; (f) lattice analysis of TEM image. Hydrothermal synthesis conditions: $Ta_2O_5/Sr(OH)_2$ = 1/1, 200 °C, 48 h.

of PEG (Ta_2O_5-1/1-ref) (Fig. 1(b)). The starting material Ta_2O_5 consisted of particles of ~200 nm in diameter (Fig. 1(a)). The larger particles indicated the further growth of Ta_2O_5 during hydrothermal treatment in $Sr(OH)_2$ solution. No growth of Ta_2O_5 was observed in the absence of $Sr(OH)_2$. Homogeneous nanorods with an average length of ~200 nm and diameter of ~25 nm were obtained (Fig. 1(c) and (d)) when $Sr(OH)_2$ and PEG were present (Ta_2O_5-1/1-48h). The TEM image in Fig. 1(e) shows the crystalline lattice along two blue lines. The interplanar spacings of 0.388 and 0.315 nm corresponded to the (0 0 1) and (1 11 0) lattice planes of orthorhombic Ta_2O_5 (JCPDF 25-0922), respectively [18]. The product morphology was the same as that of raw Ta_2O_5 when only PEG was present (not shown). The role of $Sr(OH)_2$ was thought to be inducing the growth of Ta_2O_5, and that of PEG to induce anisotropic Ta_2O_5 growth by acting as a capping agent.

XRD patterns of the products formed under different hydrothermal conditions are shown in Fig. 2. Phase-pure Ta_2O_5 (JCPDF 25-0922) was obtained after the hydrothermal treatment of Ta_2O_5 in $Sr(OH)_2$ solution in the presence or absence of PEG at a $Ta_2O_5/Sr(OH)_2$ ratio of 1/1. Diffraction peaks at 22.9°, 28.3°, 28.8°, 36.7°, 37.1°, 46.7°, 49.2°, 51.1°, and 55.5° corresponded to the (0 0 1), (1 11 0), (2 0 0), (1 11 1), (2 0 1), (0 0 2), (1 18 1), (0 9 2), and (1 11 2) lattice planes of Ta_2O_5, respectively. Additional diffraction peaks at 29.6°, 34.9°, 48.9°, and 58.2° were observed at a $Ta_2O_5/Sr(OH)_2$ ratio of 2/1, probably due to the formation of $SrTa_2O_6$ (JCPDF 51-1683).

UV-vis diffuse reflectance spectra of Ta_2O_5 prepared from different conditions are shown in Fig. 3. All samples exhibited the same UV absorption edge at ~315 nm, with negligible red or blue shifts. The corresponding band gaps of the Ta_2O_5 samples and reference Ta_2O_5 sample were ~3.9 eV, as determined from absorption onsets by plots of the square root of the Kubelka-Munk function versus photon energy [43]. This value was in agreement with that of Maeda et al. [44]. The Ta_2O_5 products

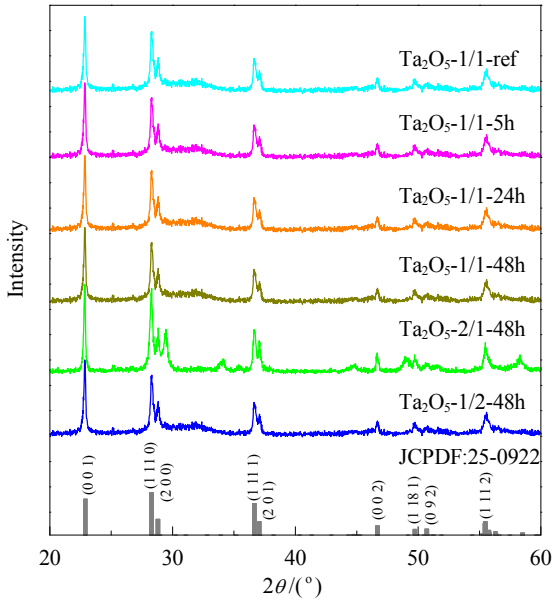

Fig. 2. XRD patterns of the products formed under different hydrothermal synthesis conditions.

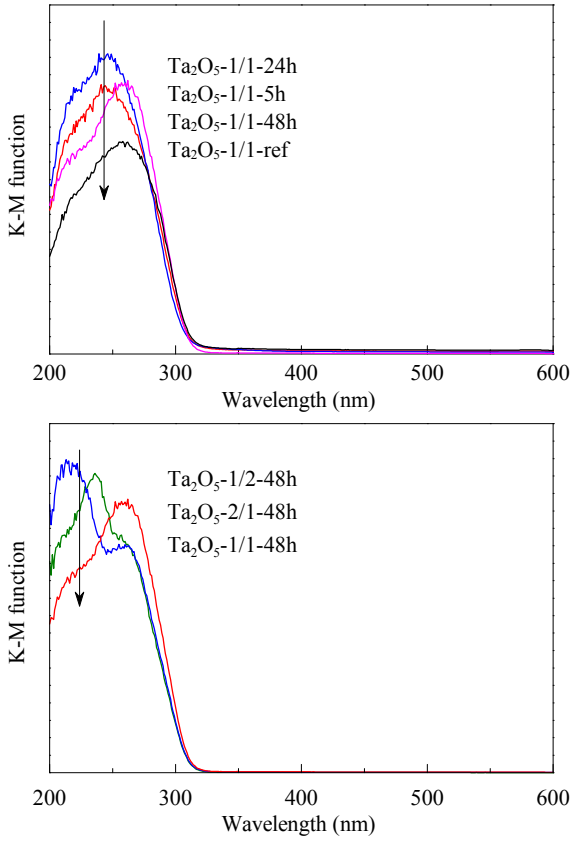

Fig. 3. UV-vis diffuse reflectance spectra of the products from different hydrothermal synthesis conditions.

were n-type semiconductors, which were expected to be photocatalytically active under UV irradiation.

3.2. *Effect of crystallization duration*

The effects of crystallization duration, $Ta_2O_5/Sr(OH)_2$ ratio, and PEG dosage on the product morphology were investigated. Figure 4(a–c) shows that the crystallization duration significantly affected the product morphology. Ta_2O_5 nanoparticles with average length-diameter ratios of 1.6, 3.6, and 8 were obtained after reaction for 5, 24, and 48 h, respectively. No further changes were observed after longer reaction durations. These observations indicated the orientated re-growth of Ta_2O_5 under hydrothermal conditions. The HRTEM image of Ta_2O_5-1/1-48h (Fig. 1(e)) indicated that re-growth occurred along the (0 0 1) plane.

3.3. *Effect of $Ta_2O_5/Sr(OH)_2$ ratio*

The $Ta_2O_5/Sr(OH)_2$ ratio affected the morphology and crystal phase of the product. Nanoparticles of mixed phase (Ta_2O_5 and $SrTa_2O_6$) were obtained at a $Ta_2O_5/Sr(OH)_2$ ratio of 2/1. Phase-pure orthorhombic Ta_2O_5 nanorods were obtained at $Ta_2O_5/Sr(OH)_2$ ratios of 1/1 and 1/2. The average length-diameter ratio of Ta_2O_5-1/2-48h nanorods was 18, higher than that of the Ta_2O_5-1/1-48h nanorods (25 × 200 nm), as shown in Fig. 4(e–f). Mixed metal oxides would be observed at $Ta_2O_5/$

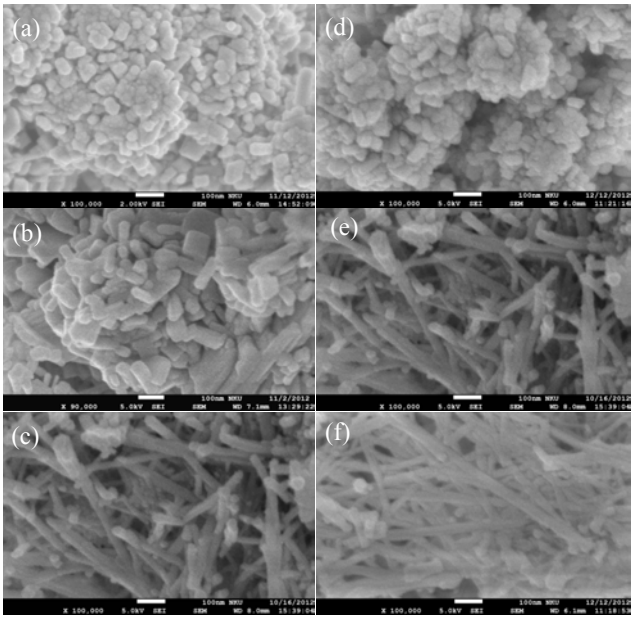

Fig. 4. SEM images of synthesis products with different reaction conditions at 200 °C. (a) Ta_2O_5-1/1-5h; (b) Ta_2O_5-1/1-24h; (c) Ta_2O_5-1/1-48h; (d) Ta_2O_5-2/1-48h; (e) Ta_2O_5-1/1-48h; (f) Ta_2O_5-1/2-48h.

$Sr(OH)_2$ ratios of < 1/2. The properties of Ta_2O_5 samples obtained from different synthesis conditions are summarized in Table 1.

3.4. Growth mechanism of Ta_2O_5 nanorods

Crystalline Ta_2O_5 is insoluble under normal conditions, even in highly alkaline media. However, Ta_2O_5 can be partly dissolved and hydroxylated to $Ta_2O_5{\cdot}xH_2O$ or $Ta(OH)_5$ at high temperature and pressure [1]. PEG has been shown to be effective for the synthesis of nanorods in metal oxide systems, such as zinc oxide [45] and cerium oxide [46].

In the present study, Ta_2O_5 in the presence of $Sr(OH)_2$ dissolved and hydroxylated to its corresponding hydroxide under hydrothermal conditions. PEG adsorbed to the resulting $Ta_2O_5{\cdot}xH_2O$ or $Ta(OH)_5$ via hydrogen bonding and van der Waals forces. The 1D PEG chains controlled the nucleation and growth of the Ta_2O_5 nanorods by favoring the formation of elongated nuclei. PEG continuously adsorbed on nuclei surfaces, with different affinities for different facets. This caused preferential growth in specific directions and the formation of 1D structure. In the presence of PEG, the growth units, i.e. the

Table 1
Properties of Ta_2O_5 samples obtained from different synthesis conditions.

Sample	BET surface area (m^2/g)	Crystal size (nm)	Crystal phase
Ta_2O_5-1/1-ref	38.0	—	Orthorhombic
Ta_2O_5-1/1-48h	27.9	25×200	Orthorhombic
Ta_2O_5-1/2-48h	46.1	25×450	Orthorhombic
Ta_2O_5-2/1-48h	10.1	30×50	Mixture
Ta_2O_5-1/1-24h	11.0	25×90	Orthorhombic
Ta_2O_5-1/1-5h	8.6	25×40	Orthorhombic

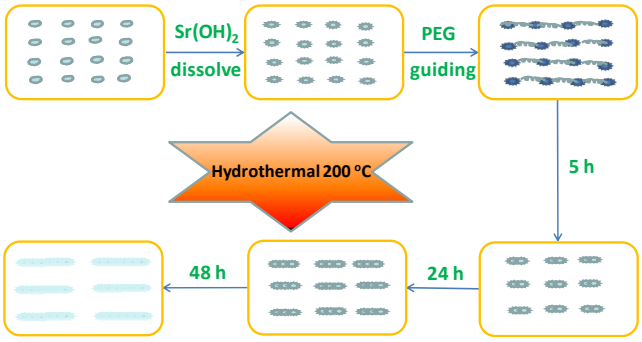

Fig. 5. Proposed formation mechanism of the Ta_2O_5 nanorods.

single Ta_2O_5 crystal lattice, preferentially landed on the (0 0 1) faces of Ta_2O_5, so nanorods gradually formed along this direction (Fig. 1). Increasing the reaction duration resulted in longer nanorods (Fig. 4). This is similar to the growth of ZnO nanorods, in which (0 0 1) is the fastest growth direction [45]. The XRD results indicated the good crystallinity of Ta_2O_5 nanorods after 5 h of hydrothermal treatment. Some irregular nanoparticles of different sizes were also formed in the absence of PEG (Fig. 1(b)). The proposed formation mechanism for the Ta_2O_5 nanorods is shown in Fig. 5.

3.5. Photocatalytic activity in RhB degradation

The photocatalytic activities of the Ta_2O_5 samples were evaluated in the degradation of RhB under UV irradiation. Dye solutions were first photolyzed in the absence of a photocatalyst to examine their stability. RhB was not degraded in the dark, and only slightly degraded under UV irradiation in the absence of a catalyst (< 2%). Thus, the photolysis and effect of catalyst adsorption were negligible. Degradation curves and corresponding plots of $\ln(C_0/C)$ versus time-on-stream (TOS) catalyzed by different samples are shown in Fig. 6. The maximum absorption of the degraded solutions exhibited hypsochromic shifts with increasing TOS. This indicated cleavage of the RhB conjugated structure, and decomposition via a series of *N*-deethylated intermediates. The degradation of RhB followed pseudo-first-order kinetics. The different Ta_2O_5 samples exhibited differing photocatalytic activities. The surface area, crystal phase, morphology, and crystallinity are the main factors affecting the photocatalytic activity of semiconductor oxides [47]. All samples (except Ta_2O_5-2/1-48h) possessed the same orthorhombic phase with similar crystallinities. Thus, the Ta_2O_5 surface area and morphology were thought to be important factors controlling the photocatalytic activity. For Ta_2O_5 nanorods of the same orthorhombic phase, the photocatalytic activity correlated well with surface area. Higher surface areas corresponded to higher apparent rate constants (k_{app}) and higher photocatalytic activity. Larger surface areas reportedly favor larger numbers of active sites, where photogenerated electron-hole pairs can induce more hydroxyl and superoxide radicals to react with organic absorbates [48]. Therefore, Ta_2O_5 nanorods with larger surface areas exhibited higher photocatalytic activity.

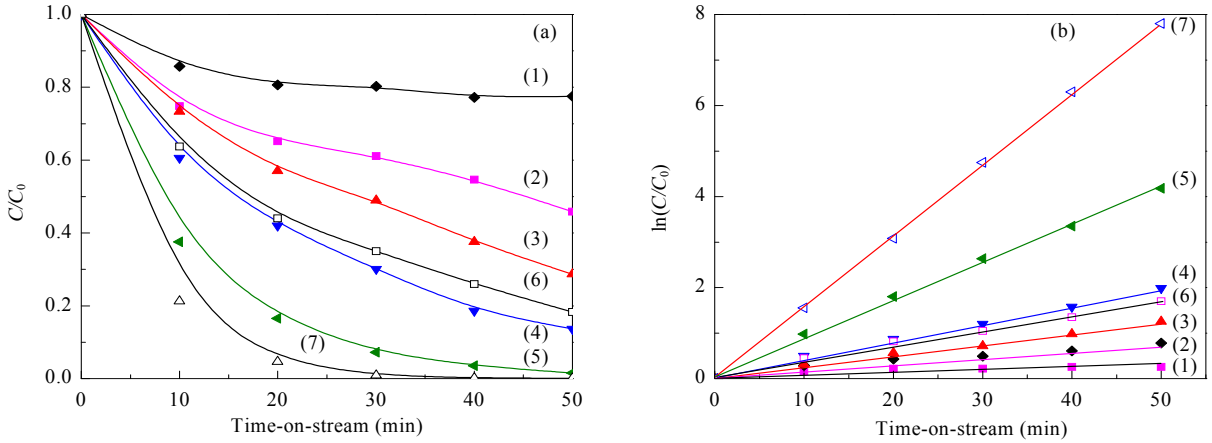

Fig. 6. Photodegradation of RhB by the Ta_2O_5 samples. (1) Commercial T_2O_5; (2) T_2O_5-1/1-ref; (3) T_2O_5-1/1-5h; (4) T_2O_5-1/1-24h; (5) T_2O_5-1/1-48h; (6) T_2O_5-2/1-48h; (7) T_2O_5-1/2-48h.

The Ta_2O_5 morphology was determined by the crystallization duration and $Ta_2O_5/Sr(OH)_2$ ratio, so both of these could be used to influence the photocatalytic activity. The lower $Ta_2O_5/Sr(OH)_2$ ratio in Ta_2O_5-*x*-48h resulted in a higher k_{app} and higher photocatalytic activity (Table 2). The highest photocatalytic activity with a k_{app} of 0.156 min^{-1} was obtained for Ta_2O_5-1/2-48h. $BaTa_2O_6$ nanorods have a reported k_{app} of 0.05495 min^{-1} [37]. Longer hydrothermal reaction durations for Ta_2O_5-1/1-*y* resulted in higher k_{app} values. Figure 7 shows a direct correlation between the length-diameter ratio and k_{app}. These observations were consistent with the reported view that 1D (nanowires and nanorods) facilitate the separation of photogenerated electron-hole pairs [49–51].

PL spectroscopy can reveal the efficiency of charge carrier trapping, immigration, and transfer in semiconductors [52,53].

Table 2
Apparent rate constants (k_{app}) for the degradation of RhB by different samples.

Sample	k_{app} (min^{-1})
Ta_2O_5-1/1-ref	0.015
Ta_2O_5-2/1-48h	0.034
Ta_2O_5-1/1-48h	0.083
Ta_2O_5-1/2-48h	0.156
Ta_2O_5-1/1-5h	0.025
Ta_2O_5-1/1-24h	0.039

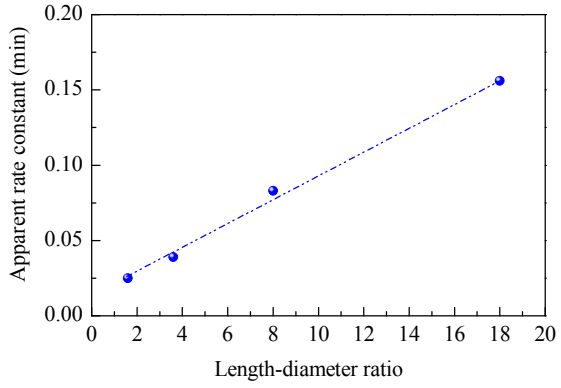

Fig. 7. Relationship between nanorod length-diameter ratio and k_{app}.

PL emission generally originates from the radiative recombination of photogenerated electrons and holes. Room temperature PL emission spectra of the Ta_2O_5 samples are shown in Fig. 8. PL peaks at 400–500 nm were observed for all samples due to surface and bulk irradiative recombination. The changes in PL intensity correlated with the observed photocatalytic activity (i.e., lower PL intensity correlated with higher photocatalytic activity).

The stability of the highest activity sample (Ta_2O_5-1/2-48h) was investigated by the successive photodegradation of RhB, as shown in Fig. 9. The photocatalyst sample was separated by centrifugation, thoroughly washed with distilled water, and

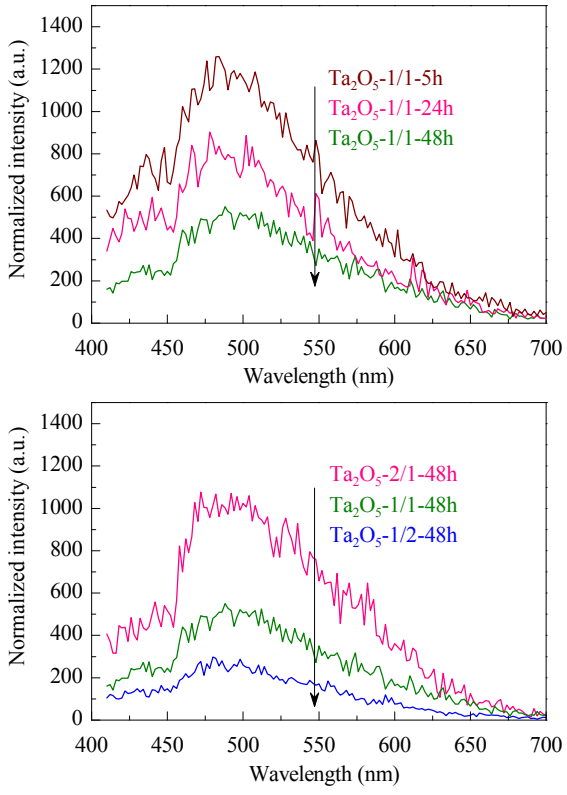

Fig. 8. PL spectra of the Ta_2O_5 samples.

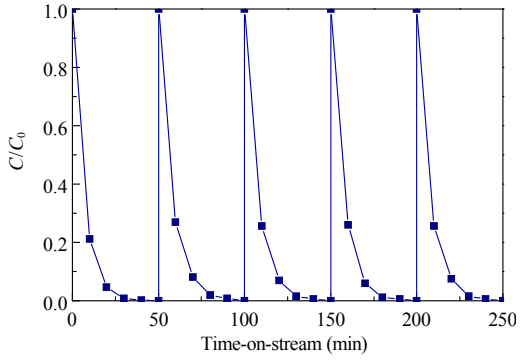

Fig. 9. Successive RhB photodegradation reactions by Ta_2O_5-1/2-48h.

then used for the subsequent photodegradation without thermal treatment. Ta_2O_5-1/2-48h exhibited good recyclability over five cycles, as evidenced by the constant photodegradation rate. Thus, Ta_2O_5-1/2-48h was stable during the photodegradation of RhB and has potential in the treatment of dye-containing waste water.

4. Conclusions

Ta_2O_5 nanorods were hydrothermally prepared from commercial Ta_2O_5. The presence of PEG and $Sr(OH)_2$ was necessary to form the nanorods. $Sr(OH)_2$ induced the surface dissolution and re-growth of Ta_2O_5. PEG induced the anisotropic growth of Ta_2O_5 by acting as a capping agent. The crystallization duration and $Ta_2O_5/Sr(OH)_2$ ratio had a strong influence on the morphology of the hydrothermal products. The Ta_2O_5 nanorods exhibited similar UV absorption properties and were used in the photodegradation of RhB under ultraviolet irradiation. The Ta_2O_5 morphology strongly affected the photocatalytic activity, and a direct correlation between the length-diameter ratio and apparent rate constant was observed. An apparent reaction rate constant of 0.156 min^{-1} was obtained for Ta_2O_5 nanorods with a length-diameter ratio of ~18. The good recyclability of the Ta_2O_5 nanorods indicated their potential for treating dye-containing waste water.

References

[1] Li X, Zang J L. *J Phys Chem C*, 2009, 113: 19411
[2] Hoffmann M R, Martin S T, Choi W, Bahnemann D W. *Chem Rev*, 1995, 95: 69
[3] Khan S U M, Al-Shahry M, Ingler W B Jr. *Science*, 2002, 297: 2243
[4] Maeda K, Teramura K, Lu D, Takata T, Saito N, Inoue Y, Domen K. *Nature*, 2006, 440: 295
[5] Chueh Y L, Chou L J, Wang Z L. *Angew Chem Int Ed*, 2006, 45: 7773
[6] Zhang J Y, Bie L J, Dusastre V, Boyd I W. *Thin Solid Films*, 1998, 318: 252
[7] Ezhilvalavan S, Tseng T Y. *J Mater Sci Mater Electron*, 1999, 10: 9
[8] Zhu Y F, Yu F, Man Y, Tian Q Y, He Y, Wu N Z. *J Solid State Chem*, 2005, 178: 224
[9] Li P, Stender C L, Ringe E, Marks L D, Odom T W. *Small*, 2010, 6: 1096
[10] Wang Y, Cui Z L, Zhang Z K. *Mater Lett*, 2004, 58: 3017
[11] Pyatenko A, Yamaguchi M, Suzuki M. *J Phys Chem C*, 2007, 111: 7910
[12] Jia C J, Sun L D, You L P, Jiang X C, Luo F, Pang Y C, Yan C H. *J Phys Chem B*, 2005, 109: 3284
[13] Chen D H, Huang F Z, Cheng Y B, Caruso R A. *Adv Mater*, 2009, 21: 2206
[14] Peng X G, Manna L, Yang W D, Wickham J, Scher E, Kadavanich A, Alivisatos A P. *Nature*, 2000, 404: 59
[15] Morales A M, Lieber C M. *Scienc*e, 1998, 279: 208
[16] Manna L, Scher E C, Alivisatos A P. *J Am Chem Soc*, 2000, 122: 12700
[17] Holmes J D, Johnston K P, Doty R C, Korgel B A. *Science*, 2000, 287: 1471
[18] Gudiksen M S, Lieber C M. *J Am Chem Soc*, 2000, 122: 8801
[19] Park S J, Kim S, Lee S, Khim Z G, Char K, Hyeon T. *J Am Chem Soc*, 2000, 122: 8581
[20] Puntes V F, Krishnan K M, Alivisatos A P. *Science*, 2001, 291: 2115
[21] Thurn-Albrecht T, Schotter J, Kästle G A, Emley N, Shibauchi T, Krusin-Elbaum L, Guarini K, Black C T, Tuominen M T, Russell T P. *Science*, 2000, 290: 2126
[22] Huang M H, Wu Y Y, Feick H, Tran N, Weber E, Yang P D. *Adv Mater*, 2001, 13: 113
[23] Lei Y, Zhang L D, Fan J C. *Chem Phys Lett*, 2001, 338: 231
[24] Urban J J, Yun W S, Gu Q, Park H. *J Am Chem Soc*, 2002, 124: 1186
[25] Ndiege N, Wilhoite T, Subramanian V, Shannon M A, Masel R I. *Chem Mater*, 2007, 19: 3155
[26] Baruwati B, Varma R S. *Cryst Growth Des*, 2010, 10: 3424
[27] Lü X J, Ding S J, Lin T Q, Mou X L, Hong Z L, Huang F Q. *Dalton Trans*, 2012, 41: 622
[28] Duan J Y, Shi W D, Xu L L, Mou G Y, Xin Q L, Guan J G. *Chem Commun*, 2012, 48: 7301
[29] Gömpel D, Tahir M N, Panthöfer M, Mugnaioli E, Brandscheid R, Kolb U, Tremel W. *J Mater Chem A*, 2014, 2: 8033
[30] Kominami H, Miyakawa M, Murakami S, Yasuda T, Kohno M, Onoue S, Kera Y, Ohtani B. *Phys Chem Chem Phys*, 2001, 3: 2697
[31] Buha J, Arcon D, Niederberger M, Djerdj I. *Phys Chem Chem Phys*, 2010, 12: 15537
[32] Devan R S, Ho W D, Lin J H, Wu S Y, Ma Y R, Lee P C, Liou Y. *Cryst Growth Des*, 2008, 8: 4465
[33] Oh M H, Lee N, Kim H, Park S P, Piao Y Z, Lee J, Jun S W, Moon W K, Choi S H, Hyeon T. *J Am Chem Soc*, 2011, 133: 5508
[34] Bonitatibus P J Jr, Torres A S, Goddard G D, Fitzgerald P F, Kulkarni A M. *Chem Commun*, 2010, 46: 8956
[35] Yu S H, Liu B, Mo M S, Huang J H, Liu X M, Qian Y T. *Adv Funct Mater*, 2003, 13: 639
[36] Hu Y M, Gu H S, Hu Z L, Di W N, Yuan Y, You J, Cao W Q, Wang Y, Chan H L W. *Cryst Growth Des*, 2008, 8: 832
[37] Xu T G, Zhao X, Zhu Y F. *J Phys Chem B*, 2006, 110: 25825
[38] Zhou C, Chen G, Li Y X, Zhang H J, Pei J. *Int J Hydrogen Energy*, 2009, 34: 2113
[39] Liu J W, Chen G, Li Z H, Zhang Z G. *Int J Hydrogen Energy*, 2007, 32: 2269
[40] Li Y X, Chen S, He H Q, Zhang Y, Wang C Y. *ACS Appl Mater Interfaces*, 2013, 5: 10260
[41] Bîrdeanu M, Bîrdeanu A V, Gruia A S, Fagadar-Cosma E, Avram C N. *J Alloys Compd*, 2013, 573: 53
[42] Zhuravleva E Y. *Inorg Mater*, 2004, 40: 671
[43] Li Z S, Yu T, Zou Z G, Ye J H. *Appl Phys Lett*, 2006, 88: 071917
[44] Maeda K, Domen K. *J Phys Chem C*, 2007, 111: 7851
[45] Liu X M, Zhou Y C. *J Cryst Growth*, 2004, 270: 527
[46] Zhang D S, Fu H X, Shi L Y, Pan C S, Li Q, Chu Y L, Yu W J. *Inorg Chem*, 2007, 46: 2446
[47] Kim S, Choi W. *J Phys Chem B*, 2005, 109: 5143

Graphical Abstract

Chin. J. Catal., 2014, 35: 432–438 doi: 10.1016/S1872-2067(14)60215-1

Hydrothermal synthesis and photocatalytic properties of tantalum pentoxide nanorods

Juxia Li, Weili Dai*, Junqing Yan, Guangjun Wu, Landong Li, Naijia Guan*
Nankai University

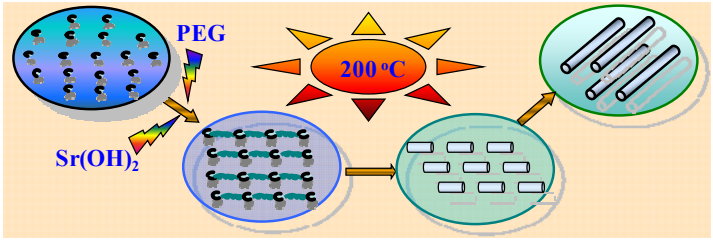

Ta_2O_5 nanorods with controllable morphology were successfully synthesized by a facile hydrothermal route in the presence of PEG and $Sr(OH)_2$. As a catalyst in the photocatalytic degradation of rhodamine B, impressive activity can be obtained over the as-synthesized nanorods.

[48] Xu N P, Shi Z F, Fan Y Q, Dong J H, Shi J, Hu M Z C. *Ind Eng Chem Res*, 1999, 38: 373
[49] Wu N Q, Wang J, Tafen D N, Wang H, Zheng J G, Lewis J P, Liu X G, Leonard S S, Manivannan A. *J Am Chem Soc*, 2010, 132: 6679
[50] Li S D, Dong Y H, Guo M R. *Appl Surf Sci*, 2012, 258: 8015
[51] Wu H B, Hng H H, Lou X W. *Adv Mater*, 2012, 24: 2567
[52] Jing L Q, Qu Y C, Wang B Q, Li S D, Jiang B J, Yang L B, Fu W, Fu H G, Sun J Z. *Sol Energy Mater Sol Cells*, 2006, 90: 1773
[53] Yan J Q, Wu G J, Guan N J, Li L D, Li Z X, Cao X Z. *Phys Chem Chem Phys*, 2013, 15: 10978

五氧化二钽纳米柱的水热合成和光催化性能

李菊霞, 戴卫理*, 闫俊青, 武光军, 李兰冬, 关乃佳#
南开大学化学学院先进能源材料化学教育部重点实验室, 天津300071

摘要: 以聚乙烯醇(PEG)为结构导向剂, 利用水热法合成了形貌可控的Ta_2O_5纳米柱. 采用X射线衍射、扫描电镜、透射电镜、漫反射紫外-可见光谱和光致发光光谱对所制备样品进行了表征. 考察了结晶时间和$Ta_2O_5/Sr(OH)_2$摩尔比等合成参数对样品形貌的影响, 并在此基础上对Ta_2O_5纳米粒可能的生长机理进行了推测. 结果表明, 在PEG和$Sr(OH)_2$存在条件下可以合成形貌可控的Ta_2O_5纳米柱. 研究了紫外光下Ta_2O_5纳米柱降解罗丹明B的光催化性能, 发现Ta_2O_5的形貌对光催化性能有很大影响, Ta_2O_5纳米柱的光催化性能与其长度和直径比成线性关系. 催化降解反应的表观速率常数最高可达0.156 min^{-1}, 且经多次循环使用后, 样品仍然保持较高的催化性能.

关键词: 五氧化二钽; 纳米结构; 晶体生长; 光催化性质; 各向异性生长

收稿日期: 2014-07-24. 接受日期: 2014-08-29. 出版日期: 2015-03-20.
*通讯联系人. 电话: (022)2359140; 传真: (022)23500341; 电子信箱: weilidai@nankai.edu.cn
#通讯联系人. 电话: (022)2359140; 传真: (022)23500341; 电子信箱: guannj@nankai.edu.cn
基金来源: 天津化学化工协同创新中心.
本文的英文电子版由Elsevier出版社在ScienceDirect上出版(http://www.sciencedirect.com/science/journal/18722067).